Covalency and spin-orbit coupling driven magnetism in the double-perovskite iridates Sr_2MIrO_6 (M = Ca, Mg)

Sayantika Bhowal[1,*] and I. Dasgupta[1,2,†]

[1]*Department of Solid State Physics, Indian Association for the Cultivation of Science, Jadavpur, Kolkata 700 032, India*

[2]*Centre for Advanced Materials, Indian Association for the Cultivation of Science, Jadavpur, Kolkata-700 032, India*

(Received 18 July 2017; revised manuscript received 10 December 2017; published 8 January 2018)

We have investigated the effect of spin-orbit coupling (SOC) and strong covalency on the magnetism of double-perovskite iridates (Sr_2MIrO_6, M = Ca, Mg) using first principles as well as model Hamiltonian calculations. Our calculation shows that strong Ir-d and O-p covalency in these double-perovskite iridates results in the deviation from the expected 6+ charge state of Ir, leading to an unquenched orbital moment in the presence of SOC. We have studied in detail the nature of magnetism and our calculations of isotropic exchange interactions for these double-perovskite iridates suggest the systems to be frustrated. We argue that the SOC driven easy plane anisotropy possibly promotes long range magnetic order suggested for these systems indicating the importance of SOC in both these systems. Further, our model calculation considering ideal d^3 electronic configuration for Ir emphasizes the role of SOC, noncubic crystal field and Ir-Ir hopping in the reduction of the spin moment.

DOI: 10.1103/PhysRevB.97.024406

I. INTRODUCTION

Recently, the important role of spin-orbit coupling (SOC) is realized in iridates [1] where the interplay between various competing parameters such as Coulomb repulsion (U), SOC (λ), Hund's Coupling (J_H), crystal field splitting (Δ_{CF}), and kinetic energy (t) gives rise to a rich variety of phases like $j_{\text{eff}} = 1/2$ Mott insulating state, [1] Weyl semimetal, [2] spin-orbital liquid state [3,4], etc. Of particular importance have been the insulating d^5 iridates, [5–8] where strong SOC renormalizes the Ir-t_{2g} orbitals into a completely filled low-lying $j_{\text{eff}} = 3/2$ quartet and a narrow half filled $j_{\text{eff}} = 1/2$ doublet which with the inclusion of moderate Coulomb repulsion opens up a gap giving rise to a $j_{\text{eff}} = 1/2$ Mott insulator.

While iridates with the charge states $Ir^{4+}(d^5)$ [5–9], $Ir^{4.5+}(d^{4.5})$ [10,11], and $Ir^{5+}(d^4)$ [4,12–15] have been investigated, iridates with the charge state $Ir^{6+}(d^3)$ hardly received any attention. This is primarily because of the prevalent notion of the quenched orbital moment in the hexavalent iridate. This scenario is, however, not true in the presence of strong SOC with the renormalized $j_{\text{eff}} = 3/2$ quartet and $j_{\text{eff}} = 1/2$ doublet. In this case the entire physics of d^3 iridates would be dictated by the $j_{\text{eff}} = 3/2$ states characterized by $|\langle L_z\rangle| = |\langle 2S_z\rangle|$ with equal magnitude but opposite direction of spin and orbital moment as shown schematically in Fig 1. In addition, the high oxidation state of Ir (Ir^{6+}) suggests the possibility of strong Ir($^{6+}$)-O chemical bonding in d^3 iridates. Hence, a unique combination of strong covalency and SOC may lead to intriguing phases in hexavalent iridates.

Jung *et al.* [16] reported the synthesis of the ordered double-perovskite systems, Sr_2MIrO_6 with M = Ca, Sr under high oxygen pressure where Ir is likely to be in $Ir^{6+}(d^3)$ charge state. The high Neel temperatures T_N = 55 K and 80 K for Sr_2CaIrO_6 (SCIO) and Sr_2MgIrO_6 (SMIO), respectively, suggest the importance of strong Ir-O covalency in these systems. A reinvestigation of these compounds [17] by x-ray absorption spectroscopy measurement further confirmed the hexavalent state of Ir in SCIO while an admixture of Ir^{6+} and Ir^{5+} is found for SMIO which is attributed to the oxygen understoichiometry in the samples. The effective magnetic moments for SCIO and SMIO as obtained from the susceptibility measurement are, respectively, 3.43 and 2.12 μ_B which are smaller compared to the spin only value (3.87 μ_B) for the d^3 configuration. The Curie-Weiss temperatures [$\Theta_{W(Sr_2CaIrO_6)} = -363.4(5)$ K and $\Theta_{W(Sr_2MgIrO_6)} = -418(1)$ K] as obtained from variation of susceptibility with temperature indicates the presence of strong antiferromagnetic (AFM) interaction in both the systems. Further, the relatively larger Θ_W compared to the ordering temperature T_N indicates the presence of frustration in both the systems which is also reflected in the divergence of zero-field-cooled (ZFC) and field-cooled (FC) data at low temperature. In spite of the presence of frustration, the neutron powder diffraction (NPD) measurement at low temperature for SCIO shows a long range canted AFM order below T_N with a propagation vector $\mathbf{q} = (1/2\ 1/2\ 0)$. While on the other hand, no long range order was detectable by NPD for SMIO, and is possibly either due to the small value of moment at the Ir site or the freezing of moments by frustration.

In view of the above mentioned experimental observations, it remains to be understood the impact of covalency, SOC and geometrical frustration in these two isostructural iridates SCIO and SMIO. In this context, first principles electronic structure calculations based on density functional theory (DFT) are an ideal tool for investigating and clarifying the electronic and magnetic properties of SCIO and SMIO. Such calculations will provide insight into the impact of Ir-O covalency, and SOC on the magnetic properties of these compounds. In fact, our calculation for both these systems shows the presence of

*sspsb3@iacs.res.in
†sspid@iacs.res.in

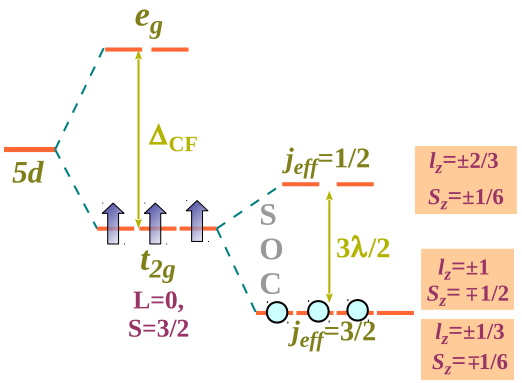

FIG. 1. Schematic diagram showing quenched orbital moment for d^3 configuration in the absence of spin-orbit coupling (SOC) while the presence of SOC leaves the orbital moment unquenched. l_z and S_z of the respective spin-orbit coupled pseudospin states are shown.

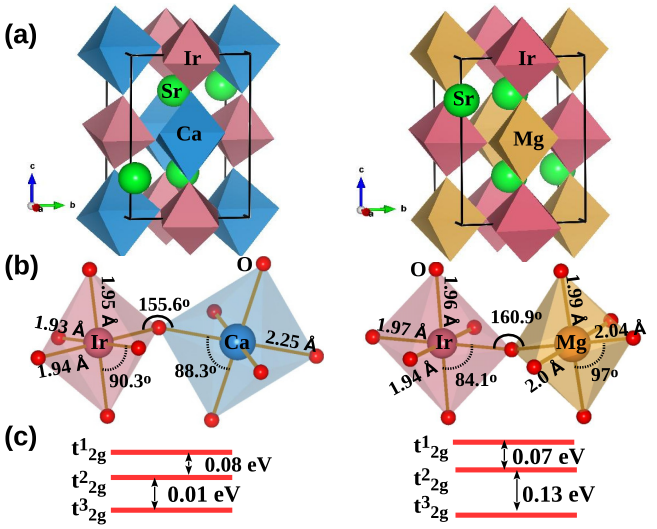

FIG. 2. (a) Structural details as follows: monoclinic structure of SCIO (left) and SMIO (right). (b) The corner-shared IrO_6 and MO_6 (M = Ca/Mg) octahedra; various bond lengths and bond angles are also marked. (c) The noncubic crystal field splitting within the t_{2g} block of Ir for SCIO (left) and SMIO (right).

ligand holes and deviation from the expected 6+ charge state of Ir ions leading to an unquenched orbital moment in the presence of SOC. In addition, we have also performed a simple single-site and two-site model Hamiltonian calculation for the ideal d^3 configuration of Ir with each site having three t_{2g} orbitals to examine the impact of the noncubic crystal field and hopping in reducing the spin moment of these systems. These results will be helpful in understanding the tunabilty of various competing parameters and hence would be useful not only to provide insights but also in the search of new materials with desired properties. The remainder of the paper is organized as follows. In Sec. II, we discuss the crystal structure of the present double-perovskite iridates, SCIO and SMIO, and our computational techniques in detail. Section III is devoted to results and discussions followed by the conclusions in Sec. IV.

II. CRYSTAL STRUCTURE AND COMPUTATIONAL DETAILS

Both SCIO and SMIO crystallize in double-perovskite monoclinic structure with the space group $P2_1/n$. [17] The crystal structure consists of corner sharing IrO_6 and MO_6 (with M = Ca, Sr) octahedra, alternating along each of the crystallographic axes as shown in Fig. 2(a). The unit cell contains two formula units with two Ir atoms in the unit cell for both the systems. The monoclinic symmetry of the structure allows the rotation of the IrO_6 octahedra with the ∠Ir-O-M ∼156° and 161°, respectively, for SCIO and SMIO. The IrO_6 octahedra are also distorted in terms of Ir-O bond length as well as ∠O-Ir-O angle. As shown in Fig. 2(b), the distortion is much more pronounced in SMIO than SCIO.

In order to study the electronic structure of these two double-perovskite iridates, DFT calculations have been performed using the plane-wave-based projector augmented wave (PAW) [18,19] method as implemented in the Vienna *ab initio* simulation package (VASP) [20,21] within the generalized gradient approximation (GGA) including Hubbard U [22] and SOC. The kinetic energy cutoff of the plane-wave basis was chosen to be 550 eV and a Γ centered 8 × 8 × 6 k mesh has been used for the Brillouin-zone integration of both the compound. All the calculations have been performed with U = 2 eV and J_H = 0.5 eV at the Ir site unless stated otherwise. In order to ascertain the accuracy of our VASP calculation, we have also performed electronic structure calculation in the full potential augmented plane-wave (FPLAPW) basis [23].

The hopping parameters as well as onsite energies of the low-energy tight-binding model retaining Ir-d-O-p and only Ir-t_{2g} in the basis are obtained from the muffin-tin orbital (MTO) based Nth order MTO (NMTO) method [24–26] as implemented in the Stuttgart code as well as by constructing the Wannier function using the VASP2-WANNIER and the WANNIER90 codes [27]. Further, we have analyzed the chemical bonding by computing the crystal orbital Hamiltonian population (COHP) as implemented in the Stuttgart tight-binding linear muffin-tin orbital (TB-LMTO) code [28]. The COHP provides the information regarding the specific pairs of atoms that participate in the bonding, while the integrated COHP (ICOHP) provides the strength of such interactions.

III. RESULTS AND DISCUSSIONS

A. Nonspin polarized electronic structure

To start with we have analyzed the electronic structure of SCIO and SMIO without any magnetic order. Though this analysis is inadequate to describe the real material, it is useful to understand the effect of magnetism and SOC successively in these iridates. The monoclinic distortion of the IrO_6 octahedra splits the Ir-t_{2g} states completely into three nondegenerate states in both the compounds. As expected from the analysis of the crystal structure for these two systems, the noncubic crystal field is stronger in SMIO than in SCIO. The calculated crystal field splitting is shown in Fig. 2(c).

The characteristic feature of the electronic structure of these two iridates is the isolated manifold of six t_{2g} bands arising from the two Ir atoms in the unit cell across the Fermi level making the system metallic within GGA. As we can see from

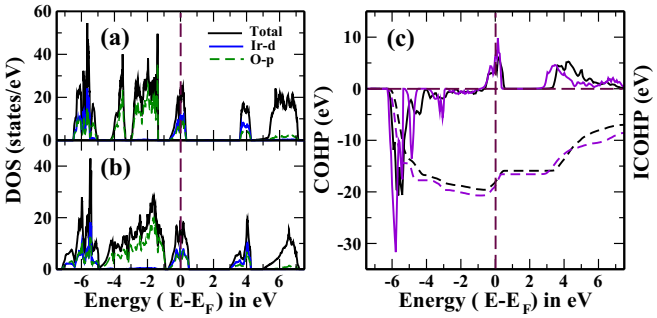

FIG. 3. Total and partial density of states for the Ir-d and O-p orbitals for (a) SCIO and (b) SMIO. (c) COHPs (solid line) and integrated COHPs (ICOHP) (dotted line) for Ir-O bonds in SCIO (maroon color) and SMIO (indigo color).

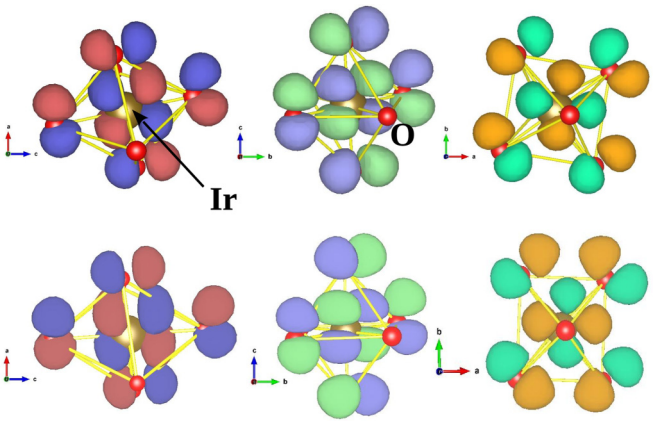

FIG. 4. Wannier function plot for Ir-t_{2g} orbitals in SCIO (top) and SMIO (bottom), respectively.

Figs. 3(a) and 3(b), the Ir-t_{2g} states are separated from the completely empty e_g states by an energy separation of ∼4 eV for both SCIO and SMIO. The Ir-t_{2g} states around the Fermi level are strongly admixed with O-p states suggesting not only strong Ir-O covalency but also the presence of ligand holes. Interestingly, the plot for the density of states (DOS) [see Figs. 3(a) and 3(b)] shows that in addition to the Ir-t_{2g} states around the Fermi level and empty Ir-e_g states, there are some Ir 5d characters present around −6 eV below the Fermi level indicating a relatively higher occupation of Ir orbitals than expected for the nominal d^3 configuration. In order to estimate the occupation of the Ir-d orbitals, we have integrated the occupied Ir-d partial DOS and find it to be 4.27/Ir and 4.48/Ir for SCIO and SMIO, respectively, and this result points to the fact that the true oxidation state of Ir is far from the nominal Ir^{6+} (d^3) state for both the compounds [29]. In addition, an estimation of on-site energies from the NMTO calculation keeping both Ir-d and O-p in the basis shows that O-p states lie above the Ir-t_{2g} states suggesting that Sr_2MIrO_6 (M = Ca, Sr) are likely to be negative charge transfer compounds [30]. It is also clear from the plot of DOS that SMIO has larger band width (BW ∼ 1.2 eV) than SCIO (∼ 1.0 eV). The larger BW implies larger hopping between the magnetic atoms in SMIO which is also consistent with the larger ordering temperature (T_N) for SMIO than SCIO.

We have already seen from the plot of partial DOS [see Figs. 3(a) and 3(b)] that there is a strong hybridization between Ir-t_{2g} and O-p orbitals for both the systems. This can further be visualized from the plot of the Wannier function for the three Ir-t_{2g} orbitals as shown in Fig. 4. It is clear from the plot, that for both SCIO and SMIO, Ir-t_{2g} orbitals form strong $pd\pi$ antibonding states with the neighboring O-p orbital indicating strong covalency between Ir-t_{2g} and O-p orbitals. Further, an energy resolved visualization of the chemical bonding between the iridium and oxygen atom can be obtained from the crystal orbital Hamiltonian population (COHP) plot as shown in Fig. 3(c). The distribution of all one-particle energies can be written as a sum of pair contributions, which is known as COHP,

$$\sum_j f_j \epsilon_j \delta(\epsilon_j - \epsilon) = \sum_{RL} \sum_{R'L'} H_{RL,R'L'} N_{RL,R'L'}(\epsilon),$$

where the sum on the left is over all the occupied one-electron eigenvalues, ϵ_j with the occupation number f_j. For the nonspin polarized case, $0 < f_j < 2$. On the other hand, the sum $\sum_{RL}$ indicates a double sum running over first all atoms R within the primitive unit cell and second over all atomic orbitals L centered on R. Thus in COHP, the DOS (N) is weighted by the Hamiltonian matrix elements (H). Further, the COHP can be classified into two parts, the on-site COHP ($R = R'$) corresponding to atomic contributions, consisting of $n \times n$ matrices for n number of the orbitals per site and off-site COHP ($R \neq R'$), emerging from bonding interactions between the atoms. Thus the off-site COHP represents the covalent contribution to bands [31]. The bonding contribution for which the system undergoes a lowering in energy is indicated by negative COHP and the antibonding contribution that raises the energy is represented by positive COHP. Thus it gives a quantitative measure of bonding. In Fig. 3(c) we have plotted the off-site COHP and the energy integrated COHP (ICOHP) per bond for the six Ir-O bonds forming the octahedral cage in both SCIO and SMIO. We gather from Fig. 3(c), the Ir-O covalency is substantially strong and found to be comparable for both SCIO and SMIO as revealed by the integrated COHP

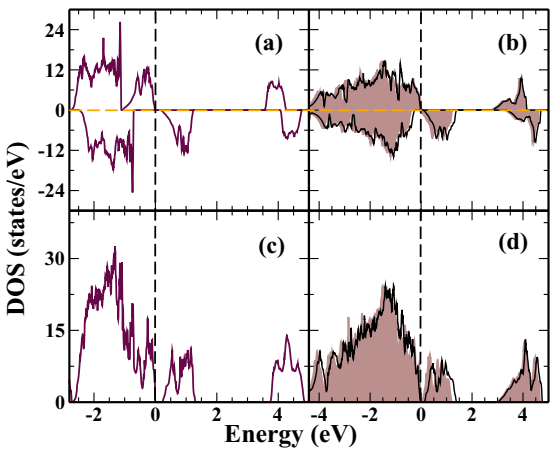

FIG. 5. The spin-polarized DOS within GGA+U (at U = 2 eV) for (a) SCIO and (b) SMIO and within GGA+SOC+U for (c) SCIO and (d) SMIO are shown. The solid black lines in (b) and (d) correspond to the DOS at U = 3 eV for SMIO.

TABLE I. The moments in the absence and presence of SOC for the FM configuration in SCIO and SMIO at $U = 2$ eV. The orbital moment at the Ir site is presented within the parentheses in the presence of SOC.

SCIO			
Configuration	Moment/Ir (orb) μ_B	Moment/O μ_B	Total Moment μ_B/fu
FM+U	1.64	0.16	3
FM+SOC+U	1.40 (−0.06)	0.14	2.59
SMIO			
Configuration	Moment/Ir (orb) μ_B	Moment/O μ_B	Total Moment μ_B/fu
FM+U	1.55	0.18	2.98
FM+SOC+U	1.17 (−0.11)	0.15	2.36

at the Fermi level. The Ir-O covalency plays a crucial role for Ir not being in the expected hexavalent state as argued earlier.

B. Magnetism and estimation of isotropic exchange interactions

In order to analyze the effect of magnetism in these two iridates we have carried out spin polarized GGA+U calculation with $U = 2$ eV and $J_H = 0.5$ eV considering the FM arrangement of Ir atoms. For the FM arrangement in SCIO, the system is insulating with a total moment of $3\,\mu_B$/fu as shown in Fig. 5(a). The situation is, however, slightly different for SMIO where there is only a pseudogap at the Fermi level for $U = 2$ eV as shown in Fig. 5(b) (see the shaded region). With the slight increase in U value (at $U = 3$ eV), a very small gap of 31 meV opens up which is visible in the DOS in Fig. 5(b) (see the solid black line). Interestingly, the moment at the Ir site for both the systems reduces appreciably (see Table I) and due to strong hybridization the oxygen atoms acquire substantial moment. In fact the moment at the Ir site is found to be smaller in the case of SMIO ($1.55\,\mu_B$) compared to SCIO ($1.64\,\mu_B$).

Next we have calculated the symmetric exchange interactions to provide insight into the geometrical frustration in these iridates. The exchange interactions are calculated up to the fifth nearest neighbor by mapping the total energies for various ordered spin states obtained within spin-polarized GGA+U calculation into the Ising model $H_{\text{spin}} = -\Sigma_{ij} J_{ij} S_i S_j$ where

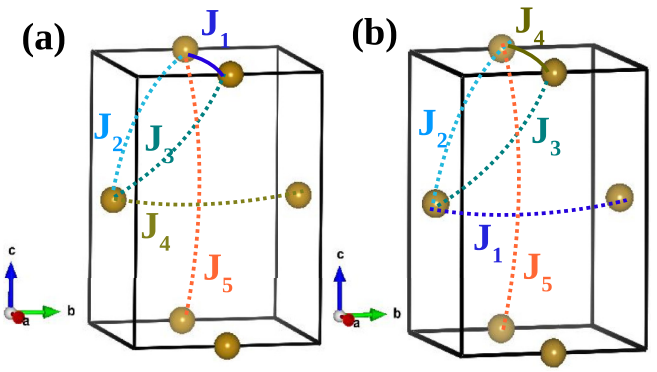

FIG. 6. Magnetic exchange interaction paths between different Ir sites are shown for (a) SCIO and (b) SMIO.

$J_{ij} < 0$ implies an AFM ground state while $J_{ij} > 0$ indicates a ferromagnetic (FM) ground state. The calculated exchange parameters for two different values of U ($U = 2$ eV and $U = 4$ eV keeping Hund's coupling $J_H = 0.5$ eV) for both SCIO and SMIO are listed in Table II.

As we can see from Table II , the 12 nearest neighbor (B-B) in an ideal cubic double perovskite $A_2B'BO_6$ splits into 2-4-4-2 neighbors due to monoclinic distortion. Thus the first four neighbors essentially form the fcc lattice for both SCIO and SMIO. Interestingly, all these interactions are AFM in nature and comparable in strength for both these iridates and hence they form a frustrated network. The AFM interaction between the Ir atoms as well as the geometrically frustrated network are in accordance with the experimental observations as discussed earlier. The different exchange paths (J_i) are indicated in Figs. 6(a) and 6(b) for SCIO and SMIO, respectively.

The Ir-Ir exchange interactions are stronger in SMIO compared to that of SCIO and is consistent with the higher ordering temperature T_N and Curie temperature Θ_W for SMIO. The stronger exchange interactions in SMIO can be understood from the relatively smaller Ir-Ir distances in SMIO as listed in Table II which is further attributed to the smaller Mg^{2+} (0.86 Å) ionic radii compared to that of Ca^{2+} (1.14 Å).

C. Effect of spin-orbit coupling on the electronic structure of SCIO and SMIO

SOC has a profound impact on magnetism. The DOS in the presence of SOC is shown in Figs. 5(c) and 5(d) for SCIO and SMIO, respectively. It is important to note that at $U = 2$ eV

TABLE II. Exchange interactions (J_i) obtained from total energy calculation within GGA+U formalism for SCIO and SMIO; negative sign implies antiferromagnetic (AFM) interaction. J_i is the interaction corresponding to the i^{th} neighbor.

Exchange interactions	SCIO			SMIO		
J_i	Distance (d_i)	J_i (meV) at		Distance (d_i)	J_i (meV) at	
(Coordination no.)	in Å	$U = 2$ eV	$U = 4$ eV	in Å	$U = 2$ eV	$U = 4$ eV
J_1 (2)	5.767	−2.6	−1.8	5.575	−7.5	−7.1
J_2 (4)	5.777	−3.1	−2.4	5.576	−6.6	−4.2
J_3 (4)	5.797	−3.3	−2.1	5.582	−4.7	−4.1
J_4 (2)	5.816	−4.5	−2.9	5.591	−3.6	−2.7
J_5 (2)	8.177	−0.5	−0.2	7.884	−0.3	−0.1

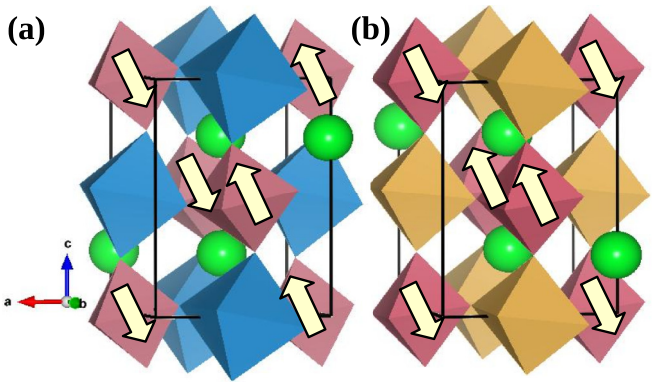

FIG. 7. The theoretically obtained magnetic ground state for (a) SCIO and (b) SMIO. See text for details.

in the presence of SOC there is no gap in the DOS for SMIO in the FM configuration. However, with increase in U (U = 3 eV), the energy gap (179 meV) appears [see the solid black line in Fig 5(d)]. Further, not only the total moment but also the moment at the Ir site is reduced to 1.4 μ_B and 1.17 μ_B for SCIO and SMIO, respectively. A small but finite orbital moment ($\sim 0.06 - 0.11\,\mu_B$) at the Ir site also appears with its direction opposite to the spin moment. The value of these small orbital moments suggests that the present iridates lie in an intermediate regime between the LS and jj coupling scheme. Thus we can see that the origin of reduction of the moment at the Ir site is twofold. While strong covalency of the Ir atom with the oxygen leading to deviation of the oxidation state of Ir from the nominal Ir^{6+} state reduces the moment at the Ir site, the presence of SOC further lowers the spin moment and a finite orbital moment is developed. Recently the importance of SOC is also realized in the resonant inelastic x-ray scattering measurements on d^3 osmates [32].

In order to understand the possible magnetic ground state of SCIO and SMIO, we have done the symmetry analysis [33]. The $P2_1/n$ symmetry of SCIO along with the experimentally reported propagation vector $\mathbf{q}$ = (1/2 1/2 0) allows only one magnetic configuration corresponding to the magnetic space group P_s-1. In this magnetic space group, Ir atoms within the ab plane are antiferromagnetically aligned while they are FM along the c direction with a net zero moment [see Fig. 7(a)]. The symmetry of the space group allows the Ir spins to be canted. Further, the total energy calculation with different spin quantization axes shows that the system has an easy plane (xz) anisotropy in confirmation with the experimentally reported magnetic structure. Indeed, the total energy calculation as listed in Table III clearly shows that this canted AFM structure is much lower in energy compared to the nonmagnetic (NM) and FM configuration. As shown in Table III, the spin moment/Ir ($=1.40\mu_B$) in this canted AFM structure is in good agreement with the value obtained from NPD [1.33(2) μ_B/Ir] [17]. The canted AFM ground state is found to be insulating for U = 2 eV with an energy gap of 0.3 eV in agreement with the experimentally observed insulating state of SCIO.

On the other hand, as already mentioned, for SMIO no long range order was detectable by NPD experiment and this was attributed to the small moment at the Ir site. We find in our calculation that the moment at the Ir site is smaller in SMIO in comparison to SCIO which is consistent with the smaller effective moment for SMIO as observed experimentally. Hence, in order to understand the magnetic ground state of the system, we have assumed the magnetic unit cell to be the same as the crystallographic unit cell. In that case the symmetry of the crystal structure allows four magnetic space groups: (i) $P2_1'/C'$, (ii) $P2_1/C'$, (iii) $P2_1'/C$, (iv) $P2_1/C$ out of which both $P2_1/C'$ and $P2_1'/C$ correspond to the NM configuration. Total energy calculation shows that, among the considered magnetic configurations, the magnetic structure corresponding to the magnetic space group $P2_1/C$ [see Fig. 7(b)] is lowest in energy with an energy gap of 72 meV. The results of our calculation are presented in Table III.

TABLE III. Energy differences and moments for various magnetic configurations for SCIO and SMIO in the presence of SOC at U = 2 eV. The orbital moment at the Ir site is presented within the parentheses.

SCIO				
Configuration	ΔE/f.u (meV)	Moment (orb) μ_B/Ir	Total moment μ_B/fu	Gap (meV)
NM	204	0.0	0.0	0
FM	43	1.40 (−0.06)	2.59	221
P_s-1	0	1.40 (−0.05)	0.0	306
SMIO				
Configuration	ΔE/f.u (meV)	Moment (orb) μ_B/Ir	Total moment μ_B/fu	Gap (meV)
NM ($P2_1/C', P2_1'/C$)	109	0.0	0.0	–
FM	69	1.17 (−0.11)	2.36	–
$P2_1'/C'$	22	1.26 (−0.03)	0.08	16
$P2_1/C$	0	1.22 (−0.08)	−0.03	72

It is interesting to note that in the absence of SOC, both $P2_1'/C'$ and $P2_1/C$ are energetically degenerate which emphasizes the important role of SOC in introducing the anisotropy in the system. The detail of these symmetry allowed magnetic structures are shown in Table IV. Similar to SCIO, SMIO also has an easy plane (xz) anisotropy. In fact, it is this easy plane anisotropy which is primarily responsible for these iridates to have a magnetically ordered state even in the presence of the geometrically frustrated AFM fcc network of Ir. Such spin-orbit-induced anisotropy is also found to be essential for long range order (type I) in d^3 osmate based double perovskite Sr_2ScOsO_6 [34].

TABLE IV. The detail of the symmetry allowed magnetic structures corresponding to SMIO assuming the propagation vector $\mathbf{q}$ = (0,0,0).

Magnetic space groups	Ir (1) (1/2,0,1/2)	Ir(2) (0,1/2,0)
$P2_1/C', P2_1'/C$	(0,0,0	(0,0,0)
$P2_1'/C'$	(m_x,m_y,m_z)	(m_x,$-m_y$,m_z)
$P2_1/C$	(m_x,m_y,m_z)	($-m_x$,m_y,$-m_z$)

D. Model Hamiltonian approach

Finally, we have employed many-body multiplet calculation embodied within the model Hamiltonian approach to understand the importance of SOC in reducing the spin moment and to illuminate the role of other relevant parameters like J_H, noncubic crystal field ($\Delta_{\rm NCF}$), and hopping (t) on magnetism in an ideal d^3 electronic configuration. In view of this, we have considered the following model Hamiltonian to describe the t_{2g} states of Ir in the ideal d^3 electronic configuration.

$$H = H^{\Delta} + H_t + H^{\rm int} + H^{\rm SO}, \tag{1}$$

where, H^{Δ}, H_t, $H^{\rm int}$, and $H^{\rm SO}$ are, respectively, the Hamiltonian for the noncubic crystal field, hopping between the three t_{2g} orbitals, Coulomb interaction, and the spin-orbit interaction.

The effect of noncubic crystal field is included by considering the term H^{Δ} in the model Hamiltonian,

$$H^{\Delta} = \sum_i H^{i,\Delta} = \sum_i \sum_{l,m=1,2,3} \sum_{\sigma} \varepsilon_{lm} d^{\dagger}_{i,l\sigma} d_{i,m\sigma}, \tag{2}$$

where ε_{lm} represents the onsite energy.

The Ir-Ir hopping is taken into account in H_t given by

$$H_t = \sum_{i \neq j} \sum_{l,m=1,2,3} \sum_{\sigma,\sigma'} t_{ij}^{l\sigma,m\sigma'} d^{\dagger}_{il\sigma} d_{jm\sigma'}, \tag{3}$$

where t_{ij} is the hopping between the two Ir sites i and j. Here, we shall consider only a two-site model assuming the hopping to be diagonal in the orbital and spin space, i.e., $t_{ij}^{l\sigma,m\sigma'} \rightarrow t_{ij}\delta_{l,m}\delta_{\sigma,\sigma'}$. This assumption does not affect the qualitative feature of the low energy physics as also discussed in Ref. [14]. The interaction part of the Hamiltonian in Eq. (1) can be written as [35]

$$\begin{aligned} H^{\rm int} &= \sum_i H^{i,\rm int} \\ &= U_d \sum_i \sum_{l=1,2,3} n_{i,l\uparrow} n_{i,l\downarrow} \\ &+ \frac{U'_d - J_H}{2} \sum_i \sum_{\substack{l,m=1,2,3 \\ (l\neq m)}} \sum_{\sigma} n_{i,l\sigma} n_{i,m\sigma} \\ &+ \frac{U'_d}{2} \sum_i \sum_{\sigma\neq\sigma'} \sum_{\substack{l,m=1,2,3 \\ (l\neq m)}} n_{i,l\sigma} n_{i,m\sigma'} \\ &+ \frac{J_H}{2} \sum_i \sum_{\substack{l,m=1,2,3 \\ (l\neq m)}} (d^{\dagger}_{i,l\uparrow} d_{i,m\uparrow} d^{\dagger}_{i,l\downarrow} d_{i,m\downarrow} + \text{H.c.}) \end{aligned} \tag{4}$$

where, U_d, U'_d, and J_H are respectively intra-orbital Coulomb interaction, inter-orbital Coulomb interaction and Hund's rule coupling. These Coulomb interactions have the relation $U_d = U'_d + 2J_H$. $d_{i,l\sigma}(d^{\dagger}_{i,l\sigma})$ is the annihilation (creation) operator of the l^{th} orbital ($l = 1,2,3$) at the i^{th} site with a spin σ and $n_{i,l\sigma} = d^{\dagger}_{i,l\sigma} d_{i,l\sigma}$.

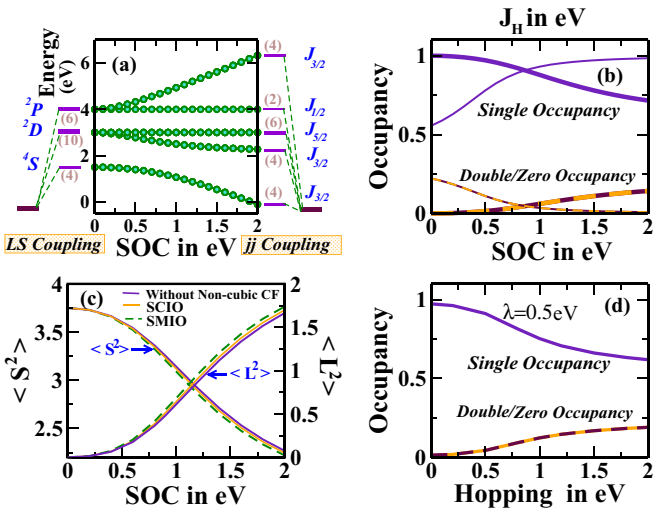

FIG. 8. (a) The evolution of energy states of $5d$ t_{2g}^3 Ir^{6+} ion calculated as a function of SOC. (b) The variation of zero (maroon), single (indigo), and double occupancy (orange) with SOC (λ) (thick line) and Hund's Coupling (J_H) (thin line). (c) The variation of expectation values of S^2 and L^2 operators with SOC in the absence (indigo) and presence of noncubic crystal field corresponding to SCIO (orange) and SMIO (green dotted). (d) The variation of zero (maroon), single (indigo), and double occupancy (orange) with hopping at a fixed value of SOC.

Finally, the explicit form of the spin-orbit interaction is given by [35]

$$H^{i,\rm SO} = \frac{i\lambda}{2} \sum_i \sum_{lmn} \epsilon_{lmn} \sum_{\sigma\sigma'} \sigma^n_{\sigma\sigma'} d^{\dagger}_{i,l\sigma} d_{i,m\sigma'}, \tag{5}$$

where λ is the magnitude of spin-orbit interaction between orbital (l) and spin (s) angular momenta of the electron and ϵ_{lmn} is the Levi-Civita symbol.

Results of exact diagonalization

In order to understand only the effect of interaction and SOC, we have first diagonalized the Hamiltonian in Eq. (1) for a single site in the absence of noncubic crystal field with three electrons defining a Hilbert space of ${}^6C_3 = 20$ basis states. The evolution of the ground state of the single-site model Hamiltonian with the increase in SOC (λ) is shown in Fig. 8(a). As we can see from Fig. 8(a), in the strong SOC regime (jj coupling regime), the ground state becomes the fourfold degenerate $J = 3/2$ state. The calculated occupancies of the ground states for various values of λ are shown in Fig. 8(b) (see the thick line) and we find that with increase in SOC the single occupancy decreases while the double occupancy increases. Note that, because of the degenerate t_{2g} orbitals, the three t_{2g} orbitals are equivalent and hence the variation of the occupancies in the three orbitals are exactly the same. Further, since the double and zero occupancy occur simultaneously, the variation of these two occupancies are identical. The single occupancy corresponds to the spin moment while the double occupancy corresponds to the orbital moment. Hence, with increase in λ, spin moment decreases

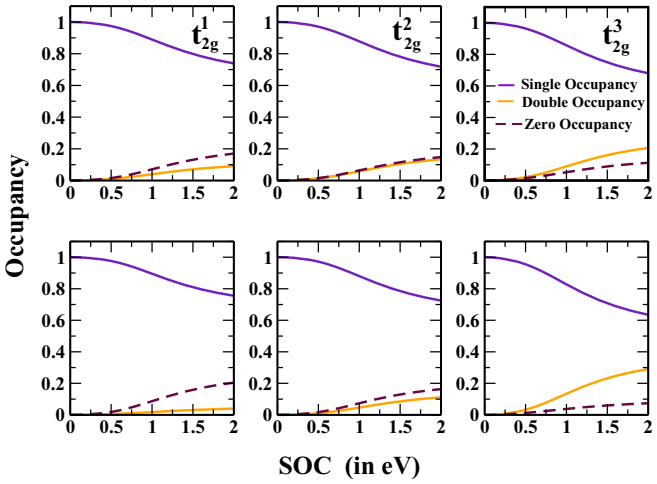

FIG. 9. The variation of zero (maroon), single (indigo), and double (orange) occupancies in the three t_{2g} orbitals with SOC in the presence of noncubic crystal field corresponding to SCIO (upper panel) and SMIO (lower panel).

from $S = 3/2$ (in the LS coupling regime) and orbital moment increases from its zero value (LS coupling regime) allowing the system to acquire a finite orbital moment. Our results are in agreement with Ref. [35] and such generation of orbital moment is also in accordance with the single particle picture where in the presence of SOC, the sixfold degenerate t_{2g} orbitals (considering spin degeneracy) are renormalized into a fourfold and a twofold degenerate energy level leaving the orbital moment unquenched.

Next, to understand the effect of Hund's coupling J_H, we have shown the variation of the occupancies (zero, single, and double occupancy) with J_H at a fixed value of λ ($\lambda = 1.5$ eV) in Fig. 8(b) (see the thin line). As we can see from the plots, single occupancy increases with J_H while double occupancy decreases. This can be attributed to the fact that J_H tries to make the spins parallel in different orbitals and thereby promotes single occupancy. Thus we can see that J_H and λ acts against each other. On the other hand, our calculation shows no dependence of the occupancies on the interorbital Coulomb interaction U'_d.

Further, to understand the impact of the noncubic crystal field on the occupancy, we have diagonalized the single-site Hamiltonian with the noncubic crystal field corresponding to SCIO and SMIO, respectively [shown in Fig. 2(c)]. In the presence of this noncubic crystal field, t_{2g} orbitals are no longer degenerate and as a result the occupancies in the three orbitals vary differently. The variation of the occupancies in each of the three orbitals with SOC is shown in Fig. 9 where the upper panel corresponds to SCIO and the lower panel corresponds to SMIO. As we can see from Fig. 9, the variation of double and zero occupancy with SOC are not identical now. This is due to the fact that because of noncubic crystal field, the lowest lying orbital t^3_{2g} prefers to be doubly occupied while the higher energy orbital t^1_{2g} prefers to be empty. Moreover, as the strength of the noncubic crystal field increases, the separation between zero and double occupancy increases. The separation between the zero occupancy and double occupancy states are larger for SMIO (see the lower panel of Fig. 9). The variation of expectation values of the L^2 and S^2 operators in the ground state with SOC in the absence and also in the presence of noncubic crystal field corresponding to SCIO and SMIO [see Fig. 8(c)], shows that the reduction of spin moment is slightly more rapid for SMIO than SCIO because of the relatively stronger noncubic crystal field in SMIO. However, the effect is not that prominent here as the difference in the noncubic crystal field between SCIO and SMIO is small (~ 0.11 eV). This clarifies that noncubic crystal field reduces the spin moment further.

Finally, to see the effect of Ir-Ir hopping in reducing the spin moment, we have considered an Ir dimer. For this purpose we have considered the Hamiltonian in Eq. (1) in the absence of noncubic crystal field and diagonalized it in the ${}^{12}C_6 = 924$ basis states forming the Hilbert space. As we can see from Fig. 8(d), at a fixed value of SOC ($\lambda = 0.5$ eV), the single occupancy decreases while the double occupancy increases with increase in hopping due to the formation of bonding and antibonding states. For the d^3 configuration, we have found from our model calculation that the interaction of Ir spins is always AFM type both in the absence and presence of SOC unlike the iridates with d^4 [4] filling where inclusion of SOC changes the interaction from FM to AFM.

IV. CONCLUSION

We have presented a detailed analysis based on first principles as well as model Hamiltonian calculation to understand the electronic structure of two isostructural double-perovskite iridates SCIO and SMIO. In contrast to the expected nominal 6+ charge state of Ir in the double-perovskite iridates Sr_2MIrO_6 (M = Ca,Mg), we find that strong Ir-d and O-p covalency gives rise to ligand holes leading to an electronic configuration of Ir far from the expected t^3_{2g} configuration. Further our calculations suggest an interesting possibility that both these iridates may be negative charge transfer compounds. The strong covalency of Ir-d and O-p orbitals is also evidenced from the plot of partial DOS, Wannier function, and COHP. Our first-principles calculation in the presence of SOC clearly shows that not only the spin moment at the Ir site decreases from the expected $S = 3/2$ value in the LS coupling regime in agreement with the experimental observation but also a small albeit finite orbital moment persists in both the double-perovskite iridates. In fact, SOC together with covalency conspire to reduce the moment at the Ir site. Further, the reduction of the moment is found to be larger in SMIO compared to SCIO in agreement with the experiment. We have also investigated the nature of magnetism of the system. The calculated exchange interactions for SCIO and SMIO clearly show the presence of geometrical frustration in both the iridates in confirmation with the experimental observation. Further, the SOC driven easy plane anisotropy helps these iridates to order magnetically.

In order to understand the role of SOC in reducing the spin moment of Ir in an ideal d^3 configuration we have considered a simple single-site and two-site model Hamiltonian. The analysis of the single-site model Hamiltonian clearly shows that with increase in SOC, the orbitals are renormalized in such a way that the single occupancy (spin moment) decreases and double occupancy (orbital moment) increases in

agreement with Matsuura *et al.* [35]. While SOC promotes double occupancy, J_H supports single occupancy thereby opposing the effect of SOC. In addition, we have found that both noncubic crystal field and Ir-Ir hopping favors double occupancy and explains the larger reduction of moments in SMIO.

ACKNOWLEDGMENTS

I.D. thanks Department of Science and Technology (DST), Government of India for support. S.B. thanks Council of Scientific and Industrial Research (CSIR), India for a Fellowship.

[1] B. J. Kim, Hosub Jin, S. J. Moon, J.-Y. Kim, B.-G. Park, C. S. Leem, Jaejun Yu, T. W. Noh, C. Kim, S.-J. Oh, J.-H. Park, V. Durairaj, G. Cao, and E. Rotenberg, Phys. Rev. Lett. **101**, 076402 (2008).

[2] Kai-Yu Yang, Yuan-Ming Lu, and Ying Ran, Phys. Rev. B **84**, 075129 (2011).

[3] T. Dey, A. V. Mahajan, P. Khuntia, M. Baenitz, B. Koteswararao, and F. C. Chou, Phys. Rev. B **86**, 140405(R) (2012).

[4] A. Nag, S. Middey, S. Bhowal, S. K. Panda, R. Mathieu, J. C. Orain, F. Bert, P. Mendels, P. G. Freeman, M. Mansson, H. M. Ronnow, M. Telling, P. K. Biswas, D. Sheptyakov, S. D. Kaushik, V. Siruguri, C. Meneghini, D. D. Sarma, I. Dasgupta, and S. Ray, Phys. Rev. Lett. **116**, 097205 (2016).

[5] S. K. Panda and I. Dasgupta, Mod. Phys. Lett. B **27**, 1350041 (2013).

[6] G. Cao, J. Bolivar, S. McCall, J. E. Crow, and R. P. Guertin, Phys. Rev. B **57**, R11039 (1998).

[7] Y. Singh and P. Gegenwart, Phys. Rev. B **82**, 064412 (2010).

[8] R. Arita, J. Kunes, A. V. Kozhevnikov, A. G. Eguiluz, and M. Imada, Phys. Rev. Lett. **108**, 086403 (2012).

[9] S. K. Panda, S. Bhowal, A. Delin, O. Eriksson, and I. Dasgupta, Phys. Rev. B **89**, 155102 (2014).

[10] S. K. Panda, S. Bhowal, Y. Li, S. Ganguly, R. Valentí, L. Nordström, and I. Dasgupta, Phys. Rev. B **92**, 180403(R) (2015).

[11] S. V. Streltsov and D. I. Khomskii, Proc. Natl. Acad. Sci. **113**, 10491 (2016).

[12] G. Cao, T. F. Qi, L. Li, J. Terzic, S. J. Yuan, L. E. DeLong, G. Murthy, and R. K. Kaul, Phys. Rev. Lett. **112**, 056402 (2014).

[13] S. Bhowal, S. Baidya, I. Dasgupta, and T. Saha-Dasgupta, Phys. Rev. B **92**, 121113(R) (2015).

[14] O. N. Meetei, W. S. Cole, M. Randeria, and N. Trivedi, Phys. Rev. B **91**, 054412 (2015).

[15] C. Svoboda, M. Randeria, and N. Trivedi, Phys. Rev. B **95**, 014409 (2017).

[16] D.-Y. Jung and G. Demazeau, J. Solid State Chem. **115**, 447 (1995).

[17] P. Kayser, M. J. Martnez-Lope, J. A. Alonso, M. Retuerto, M. Croft, A. Ignatov, and M. Teresa Fernndez-Daz, Eur. J. Inorg. Chem. **2014**, 178 (2014).

[18] P. E. Blöchl, Phys. Rev. B **50**, 17953 (1994).

[19] G. Kresse and D. Joubert, Phys. Rev. B **59**, 1758 (1999).

[20] G. Kresse and J. Hafner, Phys. Rev. B **47**, 558(R) (1993).

[21] G. Kresse and J. Furthmüller, Phys. Rev. B **54**, 11169 (1996).

[22] V. I. Anisimov, J. Zaanen, and O. K. Andersen, Phys. Rev. B **44**, 943 (1991).

[23] P. Blaha, K. Schwartz, G. K. H. Madsen, D. Kvasnicka, and J. Luitz, WIEN2K, *An Augmented Plane Wave + Local Orbitals Program for Calculating Crystal Properties* (Technische Universität, Wien, Austria, 2001).

[24] O. K. Andersen and T. Saha-Dasgupta, Phys. Rev. B **62**, R16219 (2000).

[25] O. K. Andersen, T. Saha-Dasgupta, R. W. Tank, C. Arcangeli, O. Jepsen, and G. Krier, *Electronic Structure and Physical Properties of Solids. The Uses of the LMTO Method*, Springer Lecture Notes in Physics (Springer, Berlin, 2000).

[26] O. K. Andersen, T. Saha-Dasgupta, and S. Ezhov, Bull. Mater. Sci. **26**, 19 (2003).

[27] A. A. Mostofi, J. R. Yates, Y.-S. Lee, I. Souza, D. Vanderbilt, and N. Marzari, Comput. Phys. Commun. **178**, 685 (2008).

[28] O. K. Andersen and O. Jepsen, Phys. Rev. Lett. **53**, 2571 (1984).

[29] D. J. Singh, Phys. Rev. B **49**, 1580 (1994).

[30] J. Zaanen, G. A. Sawatzky, and J. W. Allen, Phys. Rev. Lett. **55**, 418 (1985).

[31] R. Dronskowski, and P. E. Bloechl, J. Phys. Chem. **97**, 8617 (1993).

[32] A. E. Taylor, S. Calder, R. Morrow, H. L. Feng, M. H. Upton, M. D. Lumsden, K. Yamaura, P. M. Woodward, and A. D. Christianson, Phys. Rev. Lett. **118**, 207202 (2017).

[33] J. M. Perez-Mato, S. V. Gallego, E. S. Tasci, L. Elcoro, G. de la Flor, and M. I. Aroyo, Annu. Rev. Mater. Res. **45**, 217 (2015).

[34] A. E. Taylor, R. Morrow, R. S. Fishman, S. Calder, A. I. Kolesnikov, M. D. Lumsden, P. M. Woodward, and A. D. Christianson, Phys. Rev. B **93**, 220408(R) (2016).

[35] H. Matsuura and K. Miyake, J. Phys. Soc. Jpn. **82**, 073703 (2013).